This article has been published in the Journal of the Mechanical Behavior of Biomedical Materials. The final publication is available from Elsevier at https://doi.org/10.1016/j.jmbbm.2020.103726.

Response of Saos-2 Osteoblast-like Cells to Kilohertz-Resonance Excitation in Porous Metallic Scaffolds

Joseph Deering[1], Alexandre Presas[2], Bryan E.J. Lee[3], David Valentin[2], Bosco Yu[1], Christian Heiss[4,5], Kathryn Grandfield[1,3*], Wolfram A. Bosbach[4,5]

[1] Department of Materials Science and Engineering, McMaster University, Hamilton, ON, Canada

[2] Center for Industrial Diagnostics and Fluid Dynamics, Polytechnic University of Catalonia, Barcelona, Spain

[3] School of Biomedical Engineering, McMaster University, Hamilton, ON, Canada

[4] Experimental Trauma Surgery, Justus Liebig University of Giessen, Germany

[5] Department of Trauma, Hand and Reconstructive Surgery, University Hospital of Giessen, Germany

[*] Corresponding author:

Prof. Kathryn Grandfield
McMaster University
1280 Main Street West
Hamilton, ON, L8S 4L7
Canada
Email: kgrandfield@mcmaster.ca

Abstract

Post-operative therapy for joint replacement is often performed to optimize bone volume and bone-implant contact. Methods, such as pulsed therapeutic ultrasound, have been shown to be a valuable addition to regular physiotherapy to increase bone regeneration. To evaluate the efficacy of kilohertz-frequency (kHz) resonant stimuli to additively manufactured implant analogues, Saos-2 cells were seeded onto porous stainless steel scaffolds and flat substrates. Resonant frequency modes were mapped in the low kHz range, and cells were subjected to daily stimulus for 10 min at a frequency of 1.278 kHz. kHz-frequency excitation was found to increase normalized alkaline phosphatase production by almost twofold on metallic substrates relative to non-vibrated control scaffolds, while peak velocity influenced alkaline production on porous scaffolds but not flat substrates. Total cell proliferation was downregulated by excitation, and all excited samples displayed larger variability. This work indicates that vibration within the range of 0.16-0.48 mm/s

may reduce cell proliferation, but favour osteogenic gene expression. This study highlights the potential of using kHz-resonance therapy to mitigate early-onset pore occlusion to achieve uniform osseointegration through porous metallic scaffolds.

Keywords

Therapeutic ultrasound, additive manufacturing, osteoblasts, osseointegration, in vitro, proliferation, LIPUS

1. Introduction

The interaction between osteoblasts and an implant material is documented to heavily depend on the conditions in a local environment. The phenomenon of mechanotransduction, how cells transform physical forces and stresses into biochemical signals[1], is associated with change in cellular differentiation[2,3], adhesion[4,5], and morphology[6]. Cells that are key to formation of bone have previously been shown to be sensitive to mechanical stimulus in the form of vibration, where select osteogenic genes are upregulated in osteoblast-like cells cultured on two-dimensional (2D) substrates when subjected to low-frequency periodic vibrational stimulus[7,8]. Early *in vivo* work on low-frequency mechanical stimulus has shown a direct correlation between microstrain and bone remodeling[9]. Short daily stimuli with high-frequency resonant vibrations have also been observed to upregulate osteopontin, fibronectin, bone sialoprotein, and type I collagen on 2D substrates[10]. Since high-frequency therapeutic ultrasound has been shown to be effective for *in vivo* osseointegration[11], it is important to understand how three-dimensional (3D) implant materials respond to other forms of resonance across the frequency spectrum. Broad-frequency mechanical stimulus of cells cultured on porous 3D substrates, for example, has been shown to upregulate osteogenic markers such as osteocalcin and MMP-9 expression on a GAPDH-normalized basis, while maintaining similar cell counts[12]. While preliminary work in the kilohertz (kHz)-range has shown to affect *in vitro* osteoclastogenesis[13], the effect of mechanical stimulus in the kHz-range has not been substantially demonstrated on most osteogenic biomarkers.

Additive manufacturing techniques have been developed to produce porous structures for bone implants[14–16]. These low-stiffness alternatives[17,18] to traditional solid implants offer higher push-out forces[19] and mitigate stress-shielding effects and long-term bone loss[20]. However, *in vivo* work with porous scaffolds has shown a trend where newly formed bone densely populates the exterior of a scaffold[21–23] but leaves the interior less populated. Larger pores (> 210 µm) have shown to favour faster *in vivo* neovascularization and better bone-implant contact[24], but pore sizes beyond this threshold (700 µm) may show little difference in osseointegration potential[25]. Methods to modify bone growth in the 200-700 µm pore size range are needed to improve osteoconduction of bone through the interior of a porous implant.

This study aims to extend resonant stimuli to 3D printed porous scaffolds with the intent to study how this affects osteoblast-like cellular activity. Selective laser melting (SLM) was used to produce low-stiffness substrates for cell culture and laser Doppler vibrometry was used to map kHz-range resonant frequencies and energies of vibration. To our knowledge, this is the first study to attempt kHz-frequency resonant stimulation of osteoblasts cultured on additively manufactured porous specimens.

2. Methods

2.1 Lattice Fabrication

3D lattices (h = 8 mm, ⌀ = 8 mm) were generated using Autodesk Netfabb using a repeated off-axis body-centred-cubic strut configuration (Figure 1). The structures had an approximate porosity of 32% and struts with a diameter of 450 µm, resulting in a pore size of 275 µm. Geometries were fabricated by selective laser melting (SLM) of 304L stainless steel powder (<45 µm, LPW Technology Inc.) with a laser power of 200 W, layer thickness of 40 µm, hatch spacing of 80 µm, and scan speed of 800 mm/s. Scanning electron microscopy was performed with a JEOL 6610LV microscope at an accelerating voltage of 20 kV to characterize the native surface for cellular interaction.

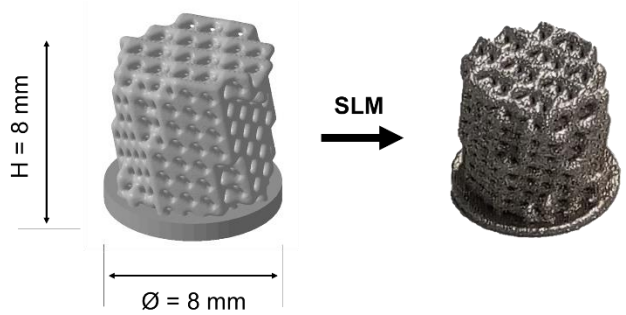

Figure 1: Comparison of input geometry and as-fabricated stainless steel geometry by SLM.

2.2 Osteoblast Culture

An osteosarcoma cell line (Saos-2, ATCC®) was used to model osteoblast behaviour on the porous metallic scaffolds. Cells were cultured in McCoy's Modified 5A media with added 15% fetal bovine serum and 1% penicillin/streptomycin (Life Technologies Inc.).

Lattices were placed into six select wells in a 24-well plate to account for nonuniform resonance modes during systemic vibration and incorporate a wide range of vibrational energy. 1.6 mL of media was added to each of the 24 wells, and the well plate was centrifuged at 200G for 6 min to eliminate air pockets from the interior of the lattice structures. Cells were detached from flasks using a solution of 0.25% trypsin-EDTA (Life Technologies Inc.) and roughly 18,000 cells were seeded on each lattice. The cell-media mixture was pipetted on to the top surface of the lattice structure.

Three plates were prepared with cells for each group: scaffolds subjected to vibration, stationary scaffolds not subjected to vibration, and cells seeded on the 24-well plate for a vibrated control on a flat substrate of tissue culture polystyrene (TCPS). Plates were incubated in 5% CO_2 at 37°C for study periods of 1 and 3 days.

An additional non-vibrated scaffold was also seeded with cells for 7 days to visualize points of focal adhesion on the porous substrates. After 7 days, cells were fixed in 0.25% glutaraldehyde and stained with osmium tetroxide before being gradually dehydrated in solutions of 50%, 70%,

70%, 95%, 95%, and 100% ethanol in Milli-Q water. Samples were critically point dried and loaded into a TESCAN VP scanning electron microscope at an accelerating voltage of 10 kV to characterize cell-material interaction.

2.3 Vibrational Stimulus

A piezoelectric transducer (PI-876-SP1, PI miCos GmbH) was fixed to a 154 mm x 104 mm x 5 mm stainless steel baseplate with epoxy and soldered to a feedback circuit, similar to what is seen in Valentin et al[26]. A signal was generated from a NI-9263 module (National Instruments) and amplified by a factor of 25. A Laser Doppler Vibrometer (LDV) (PDV-100, Polytec) was mounted on a tripod and used to map the excitation response of the scaffolds. A frequency sweep between 0 kHz and 5 kHz was forwarded to the piezoelectric transducer to map the modes of vibration at each resonant frequency in this range with the configuration shown in Figure 2.

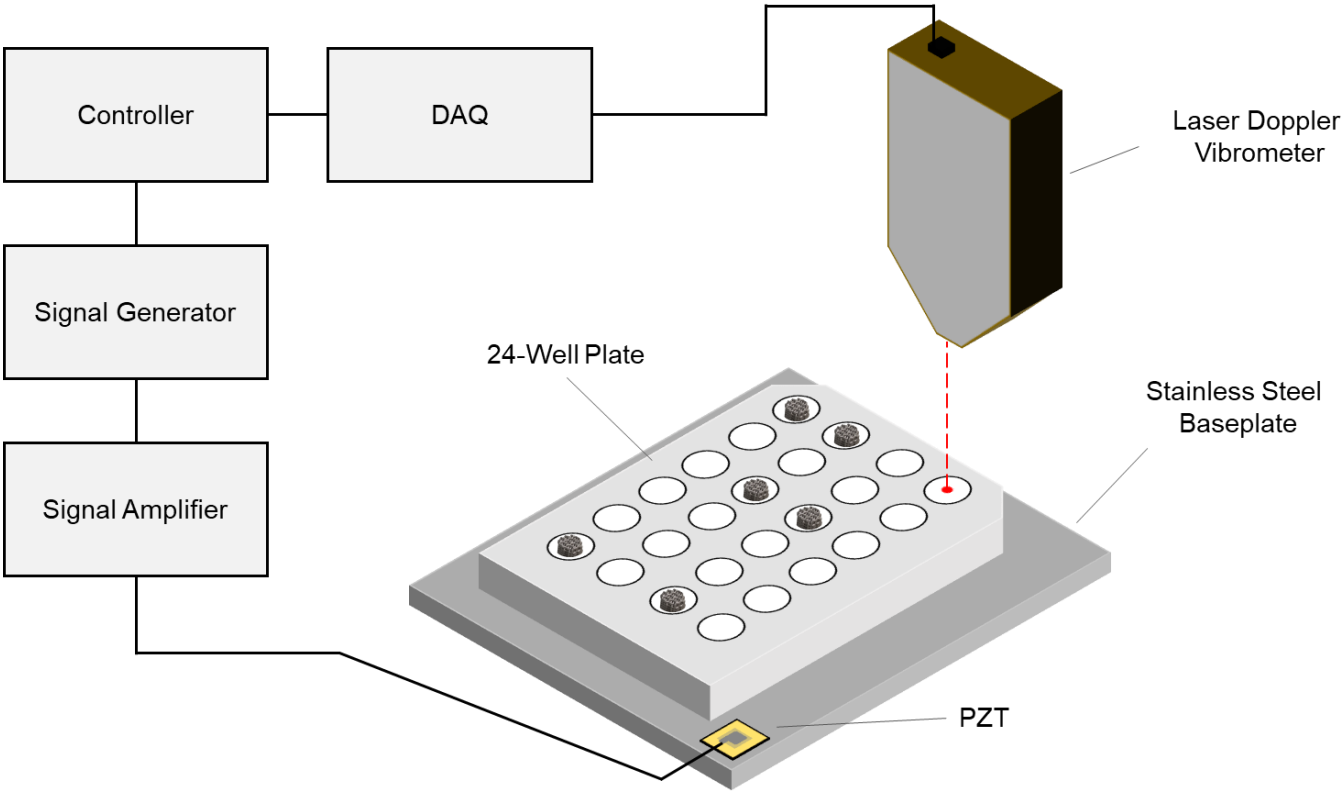

Figure 2: Bioreactor environment for application of vibrational stimulus to the plates showing locations of scaffolds. The laser doppler vibrometer measures the velocity amplitude of individual wells during the 10 min daily stimulus while the controller feeds the appropriate sinusoidal pulse to the piezoelectric transducer.

Peak energies of vibration and maximum velocities were measured with the LDV and mapped across the 24-well plate at the resonance frequencies using the corresponding mode shape. After

cells were seeded in their respective wells, scaffolds were inverted to provide a flat surface normal to the LDV to minimize laser scattering during data acquisition.

Cell culture plates were removed from the incubator and excited once daily at the chosen frequency (1.278 kHz) for 10 min, with a 24 hr rest period between vibrations. The LDV monitored the consistency of the baseplate and well vibrations by measuring the signal over the entire excitation period.

2.4 Cell Metabolism and Alkaline Phosphatase Assays

Cell metabolism was measured using alamarBlue™ reagent (Life Technologies Inc.), where resazurin is reversibly converted to fluorescent resorufin by interacting with metabolic by-products. Cell culture media was removed from the wells, and wells were rinsed with 800 µL of phosphate-buffered saline (PBS). 1.6 mL of 5% alamarBlue™ reagent in cell culture media was added to each well of interest and plates were placed back in the incubator for 60 min. The liquid was then transferred to adjacent wells to eliminate the effects of scaffold opacity. A Tecan Infinite M200 Pro plate reader was used to measure the relative fluorescence using a 540-580 nm excitation-emission wavelength. Following fluorescence, cells were lysed with a solution of 0.1% triton in PBS and culture plates were frozen at -20°C.

An alkaline phosphatase (ALP) assay was used to quantify osteoblast activity and effects of vibration on cell differentiation. 50 µL of defrosted cell lysis solution from each specimen was added to a 96-well plate in triplicate. 50 µL of a p-nitrophenyl phosphate powder dissolved in ALP assay buffer (Abcam) was added to each well, and the 96-well plate was incubated for 15 min. Absorbance readings were taken with an incident wavelength of 405 nm using a Tecan Infinite M200 Pro plate reader and converted to ALP activity using a standard calibration curve.

2.5 Statistical Analysis

A two-way ANOVA was performed in R 3.6.1 on each subset of data with Tukey's HSD to compare results. Statistical significance was assumed when $p < 0.05$. Individual datapoints were first converted to normalized ALP measurements before completing the ANOVA.

3. Results

3.1 Lattice Fabrication

The as-fabricated lattice structures had uniform pore morphology across the sample surface (Figure 3A). Measurements of pore throat diameter ranged from 220 µm to 300 µm, giving a maximum deviation from the input geometry of +35/-55 µm for these SLM conditions. On the interior of the porous structure (Figure 3B), there appeared to be no evidence of pore occlusion and bifurcations were clearly visible. Microscale and mesoscale topographical surface features were present on the surface of the specimens in the form of sintered powder particles and a melt pool solidification front. Surface topography encouraged focal adhesion, where filopodia interacted with the inherent microscale features on the surface of the lattice structure (Figure 3C). Cells tended to cluster in regions with a variety of topographic features at multiple length-scales (Figure 3D).

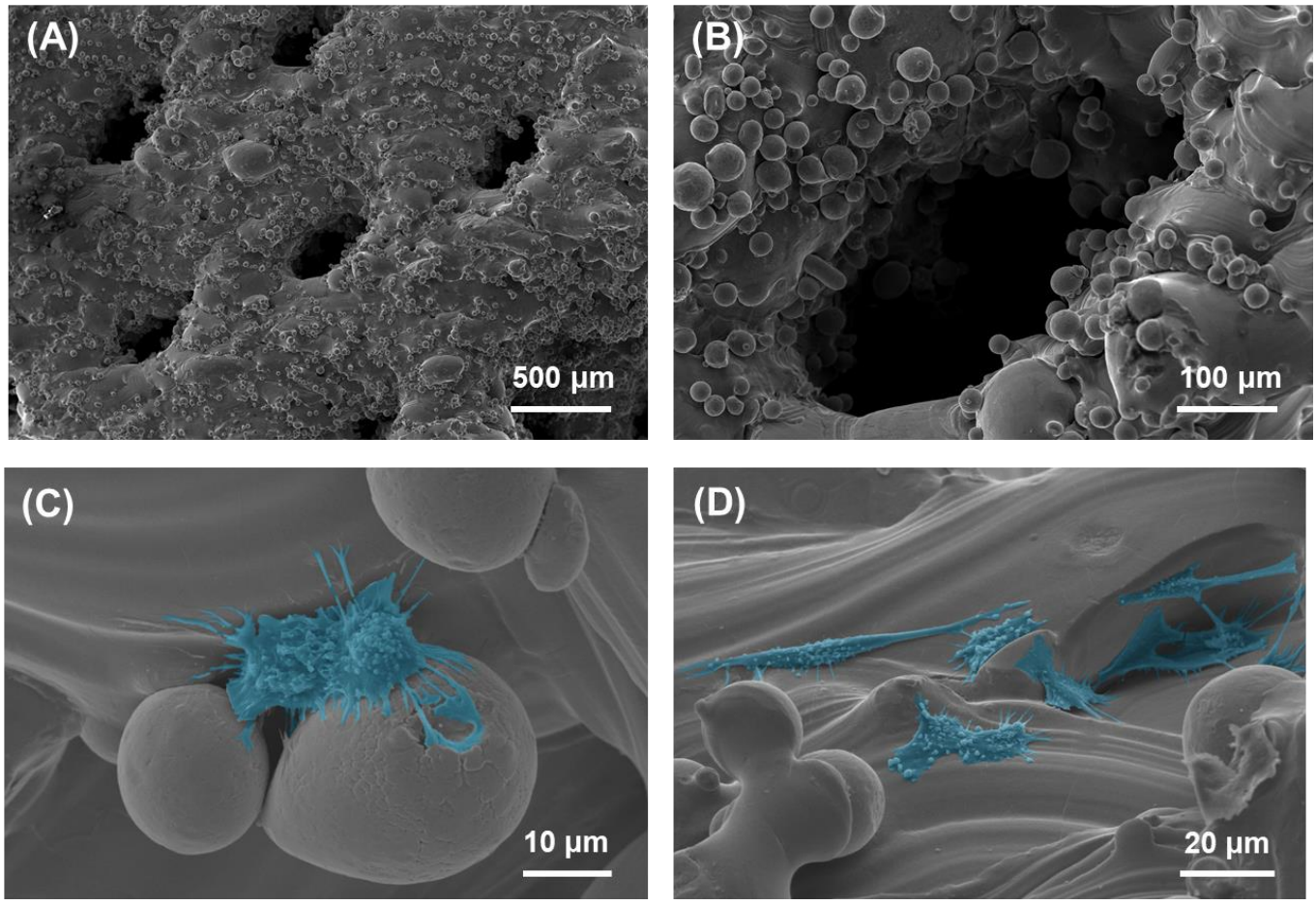

Figure 3: SEM micrographs of SLM produced stainless steel scaffolds highlighting (A) Distribution of pores across the exterior of the cylindrical specimens (B) Individual morphology of a single pore before bifurcation in the lattice structure and representative surface topography (C) Osteoblast-like cell interaction with microscale surface particles after 7 days of non-vibrated culture (D) Clustering of osteoblast-like cells around topographic areas after 7 days of non-vibrated culture.

3.2 Vibrational Stimulus

The plate was excited with a linear sweep frequency from 0-5 kHz as shown in Figure 4A. The response of the baseplate with resonant peaks is shown in Figure 4B. When measuring the dynamic response of the scaffolds in the well plate, it was observed that the connection of the well plate to the stainless steel baseplate filtered the highest resonant peaks. Nevertheless, the first natural frequency (1278 Hz) was transmitted to the well plate and to the scaffolds with a relatively high amplitude. The corresponding mode shape of this resonant peak is shown in Figure 5 and can be defined by 2 half waves along width and length of the baseplate. The amplitude of vibration (root mean square value of the velocity) varied from 0.16-0.48 mm/s depending on the scaffold location on the baseplate. Conversion to energies of vibration yield a range of 98-289 W/N depending on sampling location.

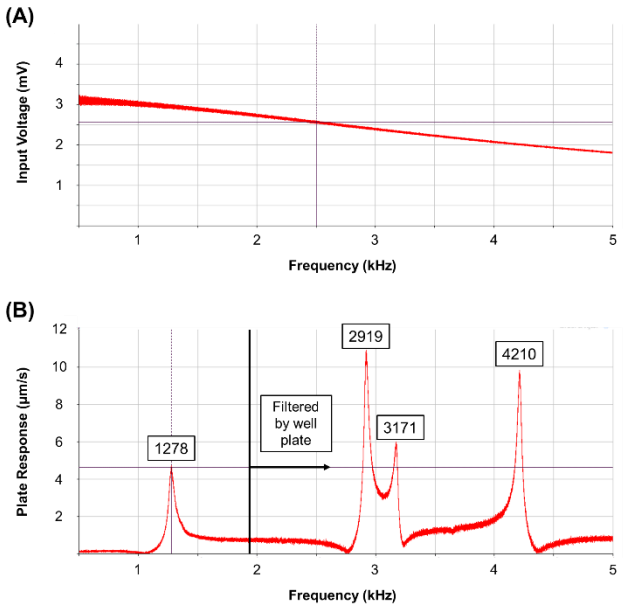

Figure 4: Results of the frequency sweep from 0-5 kHz showing (A) Excitation band of the piezoelectric transducer (B) Response of the plate at each frequency. Most resonance peaks are filtered by the in vitro culture setup. A strong signal is evident at 1.278kHz. Excitation responses are low due to the continuity of the sweep pattern.

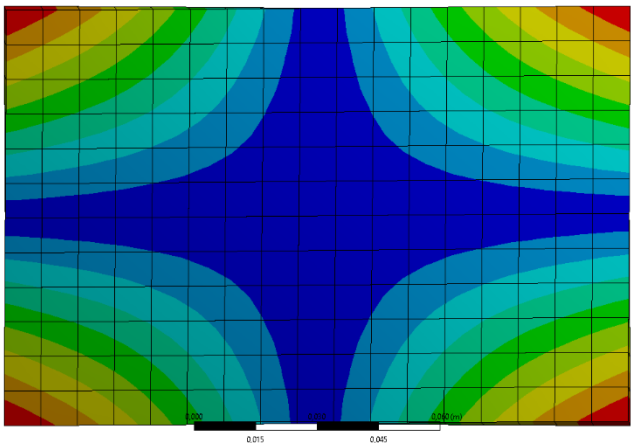

Figure 5: Mode shape of the stainless steel baseplate. The mode can be defined by two half waves along the edges of the baseplate.

3.3 Cell Metabolism and Alkaline Phosphatase Assays

Figure 6A shows the cell metabolism results for the vibrated scaffolds, vibrated control wells, and stationary scaffolds after one and three days of cell culture. A delayed response in cell proliferation is noted on both vibrated specimens from Day 1 to Day 3 compared to the stationary scaffolds ($p < 0.05$). The vibrated scaffolds show greater cell proliferation on Day 3 relative to the vibrated control specimens. ALP activity (Figure 6B) is uniform between conditions at each time point, with a slight increase in the two vibrated conditions from Day 1 to Day 3 ($p < 0.05$). Figure 6C

shows the ALP activity of each condition normalized to its corresponding cell metabolism measurement, meaning the ALP activity roughly normalized to cell number. For this normalized ALP expression, the vibrated control specimens show a greater ALP activity compared to the stationary scaffold and vibrated scaffold after 3 days *($p < 0.05$)*. In all cases, vibrated samples show a greater variance, represented by the respective ranges in the boxplots.

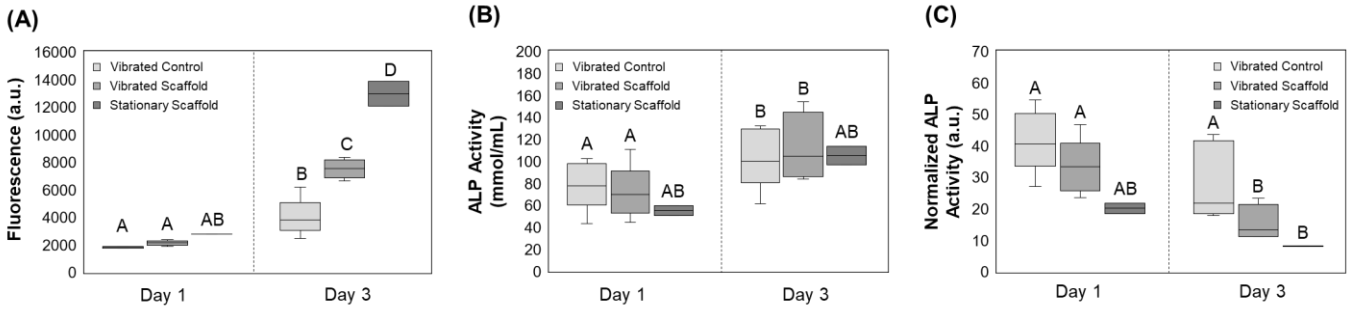

Figure 6: Osteoblast response to vibrational excitation and culture on 3D metallic scaffold showing (A) Lower cell metabolism on vibrated samples but higher cell metabolism on scaffolds relative to flat substrates (B) Similar levels of alkaline phosphatase activity across all samples (C) Elevated ALP production on a per cell basis for vibrated specimens.

Plots of fluorescence, ALP activity, and normalized ALP activity relative to the peak excitation amplitude of the individual well can be found in Figure 7, for the vibrated scaffolds and control vibrated TCPS. No trends can be discerned in terms of cell metabolism or bulk ALP production for both the scaffold and flat substrate in kHz resonance with increasing amplitude. In Figure 7E, there is an increase in normalized ALP production in the case of cells seeded on vibrated scaffolds on both Day 1 and Day 3. No such trend was replicated on the flat substrates. Normalized ALP production decreased from Day 1 to Day 3 on the porous scaffolds.

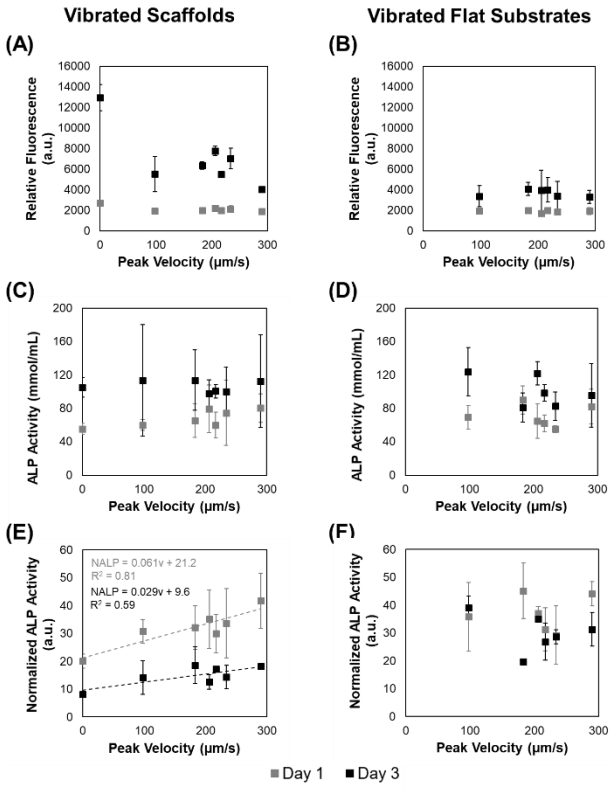

Figure 7: Effects of peak resonant velocity on cell behaviour for (A) Scaffold cell metabolism (B) Flat substrate cell metabolism (C) Scaffold ALP activity (D) Flat substrate cell metabolism (E) Scaffold normalized ALP activity (F) Flat substrate normalized ALP. ALP production on a per cell basis appears to have a slight upward trend with increased peak amplitude in the case of vibrated scaffolds but not vibrated flat substrates.

4. Discussion

The as-fabricated cylindrical specimens show no evidence of initial pore occlusion and the internal pore shape was accurate compared to the input geometry. It is important to consider the dependence of as-fabricated shape on processing parameters since strut deviations of up to 100 μm can occur in SLM of porous specimens[27,28]. For porous orthopaedic materials, *in vivo* work has shown that osseointegration is greatest when the pore throat diameter ranges from 50 μm to 400 μm[29,30]. The 275 μm diameter pores used in these experiments lie within this recommended range for optimal bone growth. Where suspended osteoblast-like cells range in diameter from 15 to 30 μm and adherent osteoblasts range in diameter from 50 to 150 μm[31], adherent and suspended osteoblasts are both free to infiltrate and proliferate through the porous network used in these tests. Maximum geometric deviations as large as 55 μm from the SLM input model were observed, however, there should be minimal influence on the ability of osteoblasts to infiltrate the structure. The SLM process inherently created native surface topography in the form of sintered surface particles and the laser solidification front. This work has shown that seeded osteosarcoma cells preferentially adhere to these surface features, with filopodia interacting in topographic regions on the surface. Dual-scale features at the microscale and nanoscale have been previously shown to increase osteoblast interaction at a biomaterial surface[32,33]. Here, the addition of dual-scale

topography in the macroscale and microscale range also showed favourable response. It is possible for the microscale surface particles to cause abrasive wear[34] at an articulating surface which may lead to increased likelihood of aseptic loosening and implant failure[35] if our scaffolds are extended to *in vivo* applications. In this case, the material may be more suitable for non-articulating surfaces. For hip implants, this may include portions that are distal to the femoral head.

In order to influence gene expression, vibrations need to translate from the excited scaffold to the cell nuclei. *In vivo*, this can be broken down into two distinct components: signal transmission from extracellular matrix to cytoskeleton, and signal transmission from cytoskeleton to nucleus[36]. Transmembrane integrin interactions bind the cell to the extracellular matrix where focal adhesions elicit an intracellular biochemical response in which kinases can be a driving force[37]. Actin filaments serve as a major part of the intermediate connection between these focal adhesions and the nuclear membrane[36]. The complex mechanism of protein interaction across the nuclear membrane of osteoblast progenitors has also previously been described[38,39], where changes in nuclear reorganization in response to externally applied forces have been observed 30 min[40] after stimulus. Therefore, it is important to account for the time-dependent response of osteoblast-like cells after excitation. In this work, vibrational stimulus was transmitted from the scaffold substrate to the nucleus and likely resulted in changes to gene expression by either nuclear motion or deformation[41]. Previous trends have been noted between vibrational stimulus and osteoblast activity for low-frequency resonance cases in the Hz range[42,43] and therapeutic ultrasound in the MHz range[44–47].

Cell metabolism increased over time for both vibrated and stationary scaffolds, as well as the control TCPS, showing that the stainless steel scaffolds are not cytotoxic across this three-day time period. Increased cell proliferation was noted for osteoblasts cultured on porous metallic scaffolds over flat substrates, which occurred despite the difference in substrate material, even though tissue culture plates typically have comparable biocompatibility to stainless steel[48]. The increased surface area in the 3D constructs allowed for better cell adhesion and proliferation, while the 3D culture environment better simulates *in vivo* conditions.

Bulk ALP expression remained statistically similar for all samples at Day 1 and all samples at Day 3. However, when normalized to cell metabolism, vibration tended to increase ALP production after 10 min of daily stimulus. This is consistent with what has been seen for other osteogenic markers such as ALP, osteocalcin, collagen type I, fibronectin, bone morphogenic proteins, Runx2, and osteopontin in the Hz and MHz range[49,50]. A decline in normalized ALP production was noted over time (between Day 1 and 3) on the vibrated scaffolds. However, since the net cell metabolism is still increasing on the vibrated scaffolds, the kHz-frequency excitation is not sufficient enough to cause extensive intrinsic cell apoptosis or necrosis. Analysis with other model cell lines and other osteogenic markers is required to determine if the osteoblast differentiation pathway has been influenced and further study should investigate the decline in normalized ALP activity over time in vibrated scaffolds.

The excitation frequency for these experiments is in the resonant range of the first natural frequency of the steel baseplate. For this type of plate (thin plate with width/length ≈ 0.66) the deformation shape is dominated by a mode shape defined by two half waves along the length and width of the plate[51]. As the vibration of the scaffolds is driven by the vibrational mode shape of the baseplate, very different amplitudes of vibration of the upper face of the scaffold have been measured with the LDV. Since the resonance mode resulted in nonuniform vibration across the

baseplate, it is also important to consider the cell response in each well rather than just the systemic biological response. An upward trend was noted for normalized ALP production with increased peak vibrational amplitude in the porous constructs, but not the flat substrates. The combinatory effects of expanded surface area on porous materials with increased excitation speed could potentially have contributed to the resulting migration and proliferation. Additional investigation into the vibration is necessary to resolve the multivariate effects on both cell viability and protein expression. While stainless steel scaffolds were used for proof of concept, the extension of these principles to other forms of additively manufactured porous biomaterials is needed. This future work should include studies with longer time periods and *in vivo* environments to validate these principles in the long-term and provide meaningful comparison to other frequency ranges in therapeutic practice.

5. Conclusions

In this work, porous metallic scaffolds were fabricated with 275 µm pores by selective laser melting of stainless steel powder. The constructs had good fidelity to the input computer model. With a maximum deviation in pore throat diameter of 55 µm, osteoblasts are easily able to infiltrate these porous structures. When placed in well-plates with cell media, a strong nonuniform resonance mode persisted in the kHz range despite filtering effects from the cell culture apparatus. Cells seeded on scaffolds and the well-plate were subjected to this daily kHz-frequency excitation. Vibrated scaffolds showed increased normalized ALP production over non-vibrated scaffolds, but lower net cell proliferation. Cells seeded on TCPS showed lower proliferation rates than metallic scaffolds, with a similar level of bulk ALP production. On a normalized basis, kHz-frequency vibration also upregulated net cell efficiency for ALP production as peak vibrational speed increased. Therefore, the application of a daily kHz-frequency resonance could offer an interesting alternative for controlled osteogenesis through 3D porous geometries and may have clinical applications in the initial post-operative stages of joint replacement, however, future work must observe this *in vivo*.

6. Acknowledgements

The authors would like to acknowledge the facilities at the McMaster University Biointerfaces Institute, McMaster University Faculty of Health Science Electron Microscopy Facility, and the Canadian Centre for Electron Microscopy. Financial support is provided by the National Sciences and Engineering Research Council of Canada, the Deutsche Forschungsgemeinschaft (DFG, grant No BO 4961/3), and by the Justus-Liebig fellowship of the Justus-Liebig University (Giessen, Germany). Alexandre Presas acknowledges the Serra Hunter program of Generalitat de Catalunya.

7. References

1. Paluch, E. K. *et al.* Mechanotransduction: use the force(s). *Bmc Biol* **13**, 47 (2015).

2. Engler, A. J., Sen, S., Sweeney, L. H. & Discher, D. E. Matrix Elasticity Directs Stem Cell Lineage Specification. *Cell* **126**, 677–689 (2006).

3. Vining, K. H. & Mooney, D. J. Mechanical forces direct stem cell behaviour in development and regeneration. *Nat Rev Mol Cell Bio* **18**, 728–742 (2017).

4. Schwartz, M. A. & DeSimone, D. W. Cell adhesion receptors in mechanotransduction. *Curr Opin Cell Biol* **20**, 551–556 (2008).

5. Iskratsch, T., Wolfenson, H. & Sheetz, M. P. Appreciating force and shape — the rise of mechanotransduction in cell biology. *Nat Rev Mol Cell Bio* **15**, 825–833 (2014).

6. Vogel, V. & Sheetz, M. Local force and geometry sensing regulate cell functions. *Nat Rev Mol Cell Bio* **7**, 265–275 (2006).

7. Ota, T., Chiba, M. & Hayashi, H. Vibrational stimulation induces osteoblast differentiation and the upregulation of osteogenic gene expression in vitro. *Cytotechnology* **68**, 2287–2299 (2016).

8. Rosenberg, N., Levy, M. & Francis, M. Experimental model for stimulation of cultured human osteoblast-like cells by high frequency vibration. *Cytotechnology* **39**, 125–130 (2002).

9. Rubin, C. T. & Lanyon, L. E. Regulation of bone mass by mechanical strain magnitude. *Calcified Tissue Int* **37**, 411–417 (1985).

10. Dumas, V. *et al.* Extracellular Matrix Produced by Osteoblasts Cultured Under Low-Magnitude, High-Frequency Stimulation is Favourable to Osteogenic Differentiation of Mesenchymal Stem Cells. *Calcified Tissue Int* **87**, 351–364 (2010).

11. Ustun, Y., Erdogan, O., Kurkcu, M., Akova, T. & Damlar, I. Effects of Low-Intensity Pulsed Ultrasound on Dental Implant Osseointegration: A Preliminary Report. *European J Dent* **02**, 254–262 (2008).

12. Tanaka, S. M. *et al.* Effects of broad frequency vibration on cultured osteoblasts. *J Biomech* **36**, 73–80 (2003).

13. Borsje, M. A., Ren, Y., de Haan-Visser, W. H. & Kuijer, R. Comparison of Low-Intensity Pulsed Ultrasound and Pulsed Electromagnetic Field Treatments on OPG and RANKL Expression in Human Osteoblast-like Cells. *Angle Orthod* **80**, 498–503 (2010).

14. Tan, X. P., Tan, Y. J., Chow, C. S. L., Tor, S. B. & Yeong, W. Y. Metallic powder-bed based 3D printing of cellular scaffolds for orthopaedic implants: A state-of-the-art review on manufacturing, topological design, mechanical properties and biocompatibility. *Mater Sci Eng C* **76**, 1328–1343 (2017).

15. Lewis, G. Properties of open-cell porous metals and alloys for orthopaedic applications. *J Mater Sci Mater Medicine* **24**, 2293–2325 (2013).

16. Dallago, M. *et al.* Geometric assessment of lattice materials built via Selective Laser

Melting. *Mater Today Proc* **7**, 353–361 (2019).

17. Wang, X., Jin-shan, L., Rui, H. & Kou, H. Mechanical properties and pore structure deformation behaviour of biomedical porous titanium. *T Nonferr Metal Soc* **25**, 1543–1550 (2015).

18. Li, X., Wang, C.-T., Zhang, W.-G. & Li, Y.-C. Properties of a porous Ti—6Al—4V implant with a low stiffness for biomedical application. *Proc Institution Mech Eng Part H J Eng Medicine* **223**, 173–178 (2009).

19. Wang, H. *et al.* The effect of 3D-printed Ti6Al4V scaffolds with various macropore structures on osteointegration and osteogenesis: A biomechanical evaluation. *J Mech Behav Biomed* **88**, 488–496 (2018).

20. Arabnejad, S., Johnston, B., Tanzer, M. & Pasini, D. Fully porous 3D printed titanium femoral stem to reduce stress-shielding following total hip arthroplasty. *J Orthopaed Res* **35**, 1774–1783 (2017).

21. Reznikov, N. *et al.* Individual response variations in scaffold-guided bone regeneration are determined by independent strain- and injury-induced mechanisms. *Biomaterials* **194**, 183–194 (2018).

22. Palmquist, A., Snis, A., Emanuelsson, L., Browne, M. & Thomsen, P. Long-term biocompatibility and osseointegration of electron beam melted, free-form–fabricated solid and porous titanium alloy: Experimental studies in sheep. *J Biomater Appl* **27**, 1003–1016 (2013).

23. de Wild, M. *et al.* Bone Regeneration by the Osteoconductivity of Porous Titanium Implants Manufactured by Selective Laser Melting: A Histological and Micro Computed Tomography Study in the Rabbit. *Tissue Eng Pt A* **19**, 2645–2654 (2013).

24. Klenke, F. M. *et al.* Impact of pore size on the vascularization and osseointegration of ceramic bone substitutes in vivo. *J Biomed Mater Res A* **85A**, 777–786 (2008).

25. Feng, B. *et al.* The effect of pore size on tissue ingrowth and neovascularization in porous bioceramics of controlled architecture in vivo. *Biomed Mater* **6**, 015007 (2011).

26. Valentín, D. *et al.* Experimental and Numerical Design and Evaluation of a Vibration Bioreactor Using Piezoelectric Patches. *Sensors* **19**, 436 (2019).

27. Han, C. *et al.* Continuous functionally graded porous titanium scaffolds manufactured by selective laser melting for bone implants. *J Mech Behav Biomed* **80**, 119–127 (2018).

28. Qiu, C. *et al.* Influence of processing conditions on strut structure and compressive properties of cellular lattice structures fabricated by selective laser melting. *Mater Sci Eng* **628**, 188–197 (2015).

29. de Vasconcellos, L., Leite, D., de Oliveira, F., Carvalho, Y. & Cairo, C. Evaluation of bone ingrowth into porous titanium implant: histomorphometric analysis in rabbits. *Braz Oral Res* **24**, 399–405 (2010).

30. Kuboki, Y., Jin, Q. & Takita, H. Geometry of carriers controlling phenotypic expression in BMP-induced osteogenesis and chondrogenesis. *J Bone Jt Surg Am Volume* **83**-A Suppl **1**, S105-15 (2001).

31. Burmester, A., Luthringer, B., Willumeit, R. & Feyerabend, F. Comparison of the reaction of bone-derived cells to enhanced MgCl 2 -salt concentrations. *Biomatter* **4**, e967616 (2014).

32. Xu, J. *et al.* Improved bioactivity of selective laser melting titanium: Surface modification with micro-/nano-textured hierarchical topography and bone regeneration performance evaluation. *Mater Sci Eng C* **68**, 229–240 (2016).

33. Gulati, K. *et al.* Anodized 3D–printed titanium implants with dual micro- and nano-scale topography promote interaction with human osteoblasts and osteocyte-like cells. *J Tissue Eng Regen M* **11**, 3313–3325 (2017).

34. Zhu, Y., Zou, J., Chen, X. & Yang, H. Tribology of selective laser melting processed parts: Stainless steel 316L under lubricated conditions. *Wear* **350**, 46–55 (2016).

35. Abu-Amer, Y., Darwech, I. & Clohisy, J. C. Aseptic loosening of total joint replacements: mechanisms underlying osteolysis and potential therapies. *Arthritis Res Ther* **9**, S6 (2007).

36. Uzer, G., Rubin, C. T. & Rubin, J. Cell Mechanosensitivity Is Enabled by the LINC Nuclear Complex. *Curr Mol Biology Reports* **2**, 36–47 (2016).

37. Biggs, M. & Dalby, M. Focal adhesions in osteoneogenesis. *Proc Institution Mech Eng Part H J Eng Medicine* **224**, 1441–1453 (2010).

38. Graham, D. M. & Burridge, K. Mechanotransduction and nuclear function. *Curr Opin Cell Biol* **40**, 98–105 (2016).

39. Bouzid, T. *et al.* The LINC complex, mechanotransduction, and mesenchymal stem cell function and fate. *J Biol Eng* **13**, 68 (2019).

40. Booth-Gauthier, E. A., Alcoser, T. A., Yang, G. & Dahl, K. N. Force-Induced Changes in Subnuclear Movement and Rheology. *Biophys J* **103**, 2423–2431 (2012).

41. Lele, T. P., Dickinson, R. B. & Gundersen, G. G. Mechanical principles of nuclear shaping and positioning. *J Cell Biol* **217**, jcb.201804052 (2018).

42. Holdsworth, D. W. *et al.* Simultaneous vibration and high-speed microscopy to study mechanotransduction in living cells. 831715-831715–6 (2012) doi:10.1117/12.913312 .

43. Shikata, T., Shiraishi, T., Morishita, S., Takeuchi, R. & Saito, T. Effects of Amplitude and Frequency of Mechanical Vibration Stimulation on Cultured Osteoblasts. *J Syst Des Dyn* **2**, 382–388 (2008).

44. Takayama, T. *et al.* Low-intensity pulsed ultrasound stimulates osteogenic differentiation in ROS 17/2.8 cells. *Life Sci* **80**, 965–971 (2007).

45. Olkku, A., Leskinen, J. J., Lammi, M. J., Hynynen, K. & Mahonen, A. Ultrasound-induced activation of Wnt signaling in human MG-63 osteoblastic cells. *Bone* **47**, 320–330 (2010).

46. Naruse, K., Miyauchi, A., Itoman, M. & Mikuni-Takagaki, Y. Distinct Anabolic Response of Osteoblast to Low-Intensity Pulsed Ultrasound. *J Bone Miner Res* **18**, 360–369 (2003).

47. Warden, S. J. *et al.* Low-Intensity Pulsed Ultrasound Stimulates a Bone-Forming Response in UMR-106 Cells. *Biochem Bioph Res Co* **286**, 443–450 (2001).

48. Bigerelle, M. & Anselme, K. Statistical correlation between cell adhesion and proliferation on biocompatible metallic materials. *J Biomed Mater Res A* **72A**, 36–46 (2005).

49. Prè, D., Ceccarelli, G., Benedetti, L., Magenes, G. & Angelis, M. Effects of Low-Amplitude, High-Frequency Vibrations on Proliferation and Differentiation of SAOS-2 Human Osteogenic Cell Line. *Tissue Eng Part C Methods* **15**, 669–679 (2009).

50. Zhang, Z. *et al.* Low-intensity pulsed ultrasound stimulation facilitates in vitro osteogenic differentiation of human adipose-derived stem cells via up-regulation of heat shock protein (HSP)70, HSP90, and bone morphogenetic protein (BMP) signaling pathway. *Bioscience Rep* **38**, BSR20180087 (2018).

51. Blevins, R. D. & Plunkett, R. Formulas for Natural Frequency and Mode Shape. *J Appl Mech* **47**, 461–462 (1980).